



Combined early dynamic ^{18}F -FDG PET/CT and conventional whole-body ^{18}F -FDG PET/CT in hepatocellular carcinoma

Yiqiu Zhang^{1,2,3,4} · Yun Dong⁵ · Wenjun Yu⁵ · Shuguang Chen^{1,3,4} · Haojun Yu^{1,3,4} · Beilei Li^{2,3,4} · Hongcheng Shi^{1,2,3,4} 

Received: 25 February 2021 / Revised: 16 November 2021 / Accepted: 17 November 2021 / Published online: 13 July 2023
© The Author(s), under exclusive licence to Springer Science+Business Media, LLC, part of Springer Nature 2023

Abstract

Objective To investigate the diagnostic value of early dynamic ^{18}F -FDG PET/CT (ED ^{18}F -FDG PET/CT) combined with conventional whole-body ^{18}F -FDG PET/CT (WB ^{18}F -FDG PET/CT) in hepatocellular carcinoma (HCC), as well as the difference of early dynamic blood flow parameters and maximum standardized uptake value (SUVmax) in HCC patients with/without liver cirrhosis or microvascular invasion (MVI).

Methods Twenty-two consecutive patients (mean age 57.8 years) with 28 established HCC lesions (mean size 4.5 cm) underwent a blood flow study with an ^{18}F -FDG dynamic scan divided into 24 sequences of 5 s each and a standard PET/CT scan. On the ED PET/CT study, an experienced PET/CT physician obtained volumes of interest (VOIs) where three blood flow estimates (time to peak [TTP], blood flow [BF], and hepatic perfusion index [HPI]) were calculated. On the WB PET/CT study, a VOI was placed on the fused scan for each HCC and maximum standardized uptake value (SUVmax) was obtained. Comparison of blood flow estimates, SUVmax, and tumor/background ratio (TNR) was performed among HCCs with and without angioinvasion, as well as HCCs in cirrhotic and non-cirrhotic liver.

Results Compared with WB ^{18}F -FDG PET/CT alone, ED combined with WB ^{18}F -FDG PET/CT can significantly increase the detection rate of moderately differentiated and poorly differentiated HCCs (both $P < 0.05$). HPI was higher in HCCs in patients with liver cirrhosis than those without liver cirrhosis ($P = 0.044$). There was no significant difference in TTP, BF, SUVmax, or TNR between HCCs in patients with liver cirrhosis and those without liver cirrhosis. There was no significant difference in blood flow estimates or SUVmax in background liver parenchyma between patients with and those without cirrhosis. TTP was shorter in HCCs with MVI than without MVI ($P = 0.046$). There was no significant difference in BF, HPI, SUVmax, or TNR between HCCs with MVI and without MVI. There was no significant difference in blood flow estimates or SUVmax in background liver parenchyma between patients with and those without MVI.

Conclusion ED combined with WB ^{18}F -FDG PET/CT can significantly increase the detection rate of moderately differentiated and poorly differentiated HCCs. HPI was significantly higher in HCCs in patients with liver cirrhosis than those without liver cirrhosis. TTP was significantly shorter in HCCs with MVI than without MVI.

Keywords Hepatocarcinoma · Early dynamic ^{18}F -FDG PET/CT · Liver cirrhosis · Microvascular invasion

Introduction

Hepatocellular carcinoma (HCC) accounts for the majority of the primary liver cancers. Globally, HCC is the fourth leading cause of cancer-related deaths and the sixth in the number of new cases. The morbidity and mortality caused by HCC in China rank the first in the world. Most HCC occurs in patients with underlying liver disease. Cirrhosis

of any cause will increase the risk of HCC. The annual incidence of HCC in patients with cirrhosis is 2–4% [1]. Conventional ^{18}F -fluorodeoxyglucose (FDG) positron emission tomography (PET)/CT imaging has obvious advantages in HCC staging, restaging, and prognostic evaluation. For the diagnosis of HCC, the positive detection rate is only about 50%; therefore, false-negative results are prone to appear, especially for the diagnosis of better differentiated HCC [2]. ^{18}F -FDG PET/CT early dynamic (ED) imaging essentially reflects the blood perfusion at the initial stage of ^{18}F -FDG entering the human tissue structure through the vein. It can be used to evaluate the blood perfusion characteristics of

Beilei Li and Hongcheng Shi have equally contributed to this work.

Extended author information available on the last page of the article

HCC lesions [3–5] and can be used as an alternative examination method for HCC patients with contraindications in enhanced CT or other enhanced imaging examinations [6]. Microvascular invasion (MVI) is defined as the presence of micrometastatic HCC emboli in hepatic vessels. Among a variety of prognostic factors, it is increasingly recognized that the presence of MVI can reflect the enhanced ability of HCC local infiltration and distant metastasis and is a key determinant of early recurrence and survival. However, at present, MVI can only be identified by histopathological studies on the excised surgical specimens [7, 8]. In this study, taking the postoperative pathology as the “gold standard,” we investigated the diagnostic value of ^{18}F -FDG PET/CT of early dynamic hepatic perfusion combined with whole-body PET/CT imaging in the diagnosis of HCC, as well as the difference of early dynamic blood flow parameters and the maximum standardized uptake value (SUVmax) in HCC patients with/without liver cirrhosis or MVI.

Materials and methods

Patients

From May 2015 to April 2017, there were 22 HCC patients (mean age 57.8 ± 9.7 years; range 34–74 years; 19 males and 3 females), with a total of 28 cancer foci. Among them, 21 patients were new cases and 1 patient was postoperative recurrence; 17 patients had a single lesion, 4 patients had 2 lesions, and 1 patient had 3 lesions. Twenty patients had a history of hepatitis B, one patient had hepatitis C, and one patient had no clear history of hepatitis. All pathological results of lesions were obtained after partial hepatectomy, liver transplantation, or liver puncture, and the pathological diagnoses were confirmed as HCCs. Among them, the pathological diagnosis of 1 lesion in a patient with liver puncture in our hospital only indicated the tumor differentiation and did not provide information on MVI and cirrhosis. The pathological results of the 3 cancer foci of the 2 patients were obtained in other hospitals and none of them provided information on tumor differentiation, MVI, or cirrhosis. The average maximum diameter of all lesions was 4.5 ± 3.2 cm (1.0–13.0 cm). This study was approved by Ethics Committee of Zhongshan Hospital, Fudan University.

Imaging protocol

^{18}F -FDG was provided by Shanghai Atom Kexing Pharmaceutical Co., Ltd, China, with radiochemical purity of $> 95\%$. All the examinations were performed on an integrated PET/CT scanner (Discovery ST, GE Healthcare, USA). The protocol included two PET/CT acquisitions: an ED PET PET/CT acquisition and a conventional WB PET/CT scan.

After the patient fasted for more than 6 h and the blood glucose was verified (< 11.0 mmol/L), a low-dose CT scan (120 kV, 80 mA) was performed, including a single bed position and centering on the liver. Then an ED ^{18}F -FDG PET scan (continuing for 120 s, consisting of 24 sequential frames of 5 s each) and the ^{18}F -FDG bolus were simultaneously performed. ^{18}F -FDG (4.44 MBq/kg) was manually administered in a 2-mL bolus in 0.9% saline as soon as possible and was followed by rinsing with 10-mL 0.9% saline.

The WB ^{18}F -FDG PET/CT scanning region encompassed the base of the skull to the proximal thigh. Parameters for helical CT image acquisition were as follows: tube voltage, 120 kV; modulated tube current–time product, 140 mAs; section thickness, 3.75 mm; and pitch, 0.516. The PET scan was performed for 2 min in each bed position, usually including 6–8 beds. CT data were used to perform attenuation correction on PET images. Datasets from PET images were reconstructed iteratively using a row-action maximum likelihood algorithm, including segmented correction for attenuation using the CT data. The images were reconstructed and displayed in three dimensions (axial, sagittal, and coronal).

Data processing and analysis

ED ^{18}F -FDG PET/CT

The ^{18}F -FDG PET images of all patients were fused with the liver-enhanced MRI or enhanced CT images performed in our hospital within the previous week by Matlab 2014a software (Mathworks Inc., USA). An experienced PET/CT physician outlined the volume regions of interest (VOI) of HCC, liver background, spleen, and abdominal aorta on the fusion images.

Reference to the literature [3], time–activity curves were generated from the mean activities for each VOI. Three blood flow parameters (i.e., time to peak [TTP], blood flow [BF], and hepatic perfusion index [HPI]) related to the first-pass delivery of FDG were derived for the HCC lesion and the background liver parenchyma, and TTP and PI were calculated for the spleen parenchyma.

Gamma-variate fit was used to correct for arterial recirculation and to locate the tissue peak of activity for noisy samples. The basic gamma-variate function is defined as follows:

$$y(t) = At^\alpha \exp\left(-\frac{t}{\beta}\right)$$

It can be shown that this expression is equivalent to the following:

$$y(t) = y_{\max} \left(\frac{t}{t_{\max}} \right)^\alpha \exp \left[\alpha \left(1 - \frac{t}{t_{\max}} \right) \right], t > 0$$

where $A = y_{\max} t_{\max}^{-\alpha} \exp(\alpha)$, $\beta = t_{\max}/\alpha$, and y_{\max} are the maximum values and t_{\max} is the time for the maximum.

If the function begins at $t = t_0 (0 \leq t_0 < t_{\max})$, we will obtain the following:

$$y(t) = y_{\max} \left(\frac{t - t_0}{t_{\max} - t_0} \right)^\alpha \exp \left[\alpha \left(1 - \frac{t - t_0}{t_{\max} - t_0} \right) \right], t > 0$$

Time to peak (TTP)

HCCs are mainly nourished by arterial blood. During the first pass, the arterial flow reaches its peak before the portal flow. Therefore, the TTP is a discriminative quantity between HCCs and liver background tissue. The following equations were used: $TTP = t_{\max} - t_a$, t_{\max} is the time at which the region of interest reaches its peak, and t_a is the time of the aorta peak.

First-pass model for measurement of blood flow (BF)

The concept of measuring tumor blood flow from the first pass of ^{18}F -FDG is based on the first-pass model of Mullani et al. [3, 9, 10]. This model is based on the hypothesis that during the first transit of a bolus of activity through an organ (or a tumor), there exists a period during which the tracer has not left the region of interest, so that the venous concentration of the tracer is extremely small. This delay time is longer with highly extracted tracers. Thus, on the base of this assumption, the tissue blood flow can be estimated using the following equation:

$$BF = \frac{Q(T)}{E(T) \cdot \int_0^T C_a(t) dt}$$

where $Q(T)$ is the residual amount of the tracer in sampled tissue at any time T , $C_a(t)$ is the arterial concentration of the tracer, and $E(T)$ is the extraction fraction.

Mullani et al. [3, 9, 10] compared the extraction fraction of ^{18}F -FDG in tumor tissue with the extraction fraction of the gold standard tracer ^{15}O -water. They found that ^{18}F -FDG extraction in tumors was close to ^{15}O -water extraction, averaging only 14% less. Thus, assuming that the first-pass extraction fraction of ^{18}F -FDG is close to 1, the expression for tumor blood flow estimates can be simplified as following:

$$BF = \frac{Q(T)}{\int_0^T C_a(t) dt}$$

A typical selection of T is when the tissue reaches peak intensity (PI). Tumor blood flow was then calculated in mL/min/g of tumor.

Hepatic perfusion index (HPI)

HPI is the percentage of arterial supply in the total liver blood supply [11]. It can be measured using the arterial first-pass slope, $dC_{\text{art}}(t)$, and portal first-pass slope, $dC_{\text{port}}(t)$, as follows:

$$HPI = \frac{\left. \frac{dC_{\text{art}}(t)}{dt} \right|_{t_{\max}}}{\left. \frac{dC_{\text{art}}(t)}{dt} \right|_{t_{\max}} + \left. \frac{dC_{\text{port}}(t)}{dt} \right|_{t_{\max}}}$$

The PI of the spleen was used to distinguish between the arterial and the portal flows.

WB ^{18}F -FDG PET/CT

An experienced PET/CT physician outlined the VOI of HCCs and liver background on the PET/CT fusion image, measured SUVmax, and calculated the tumor/background ratio (TNR).

Pathological analysis

Tumor specimens were fixed in 4% formalin, embedded in paraffin, and sliced into 4- μm -thick serial sections. Slices were analyzed by hematoxylin–eosin (H&E) staining to assess liver cirrhosis, tumor differentiation, and tumor MVI. MVI was classified into three grades according to the number and distribution of MVI: M0, no MVI; M1 (the low-risk group), ≤ 5 MVI in adjacent liver tissue ≤ 1 cm away from the tumor; and M2 (the high-risk group), > 5 MVI or MVI in liver tissue > 1 cm away from the tumor [7, 12]

Statistical analysis

The data were computed using SPSS 22.0 software (SPSS Inc., Chicago, IL, USA). Data were expressed as the average \pm standard deviation. Two independent sample t tests were used for statistical analysis for comparison between groups. A p -value of less than 0.05 was considered statistically significant for all the analyses.

Results

Visual analysis

Among 28 HCCs, 11 lesions showed high ^{18}F -FDG perfusion and metabolism (Fig. 1), 10 lesions only showed high

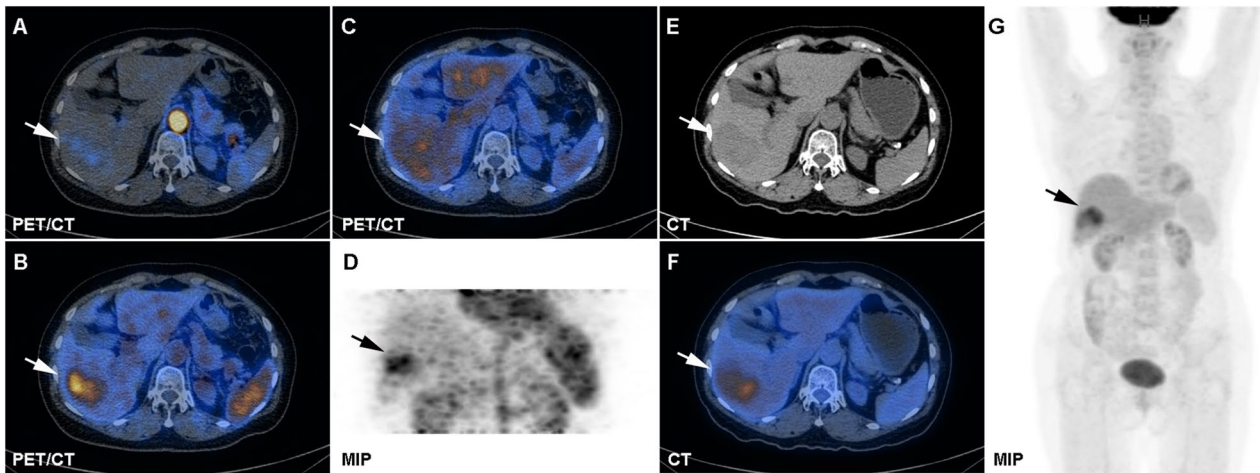


Fig. 1 A 61-year-old woman with HCC in the right lobe of the liver. The postoperative pathological diagnosis was HCC (grade III), MVI (M0), and non-cirrhosis. Axial-fused ED ^{18}F -FDG PET/CT sequential blood flow images during **a** early arterial phase, **b** late arterial phase, and **c** venous phase and **d** MIP image show preferential arterial supply to HCC (arrow) versus background liver parenchyma.

For HCC and background liver parenchyma, TTPs were 30.31 and 58.16 s, respectively; BFs were 0.74 and 0.69 mL/min/g, respectively; and HPIs were 0.57 and 0.49, respectively. WB PET/CT: axial CT, **f** fused PET/CT, and **g** PET MIP of the tumor (arrows) show increased FDG uptake in the HCC versus the background liver parenchyma (SUV_{max} = 6.4, TNR = 2.2)

^{18}F -FDG perfusion without significant ^{18}F -FDG metabolism increase (Fig. 2), 1 lesion showed only high ^{18}F -FDG metabolism but no significant increase in ^{18}F -FDG perfusion (Fig. 3), and 6 lesions had no significant increase in ^{18}F -FDG perfusion or metabolism.

Among the 11 moderately differentiated HCCs, the positive rates of ED ^{18}F -FDG PET/CT, WB ^{18}F -FDG PET/CT, and ED + WB ^{18}F -FDG PET/CT were 72.7% (8/11),

36.4% (4/11), and 72.7% (8/11). Among the 14 poorly differentiated HCCs, the positive rates of ED ^{18}F -FDG PET/CT, WB ^{18}F -FDG PET/CT, and ED + WB ^{18}F -FDG PET/CT were 71.4% (10/14), 42.9% (6/14), and 78.6% (11/14). Compared with WB ^{18}F -FDG PET/CT alone, ED + WB ^{18}F -FDG PET/CT can significantly increase the detection rate of moderately differentiated and poorly differentiated HCC (both $P < 0.05$).

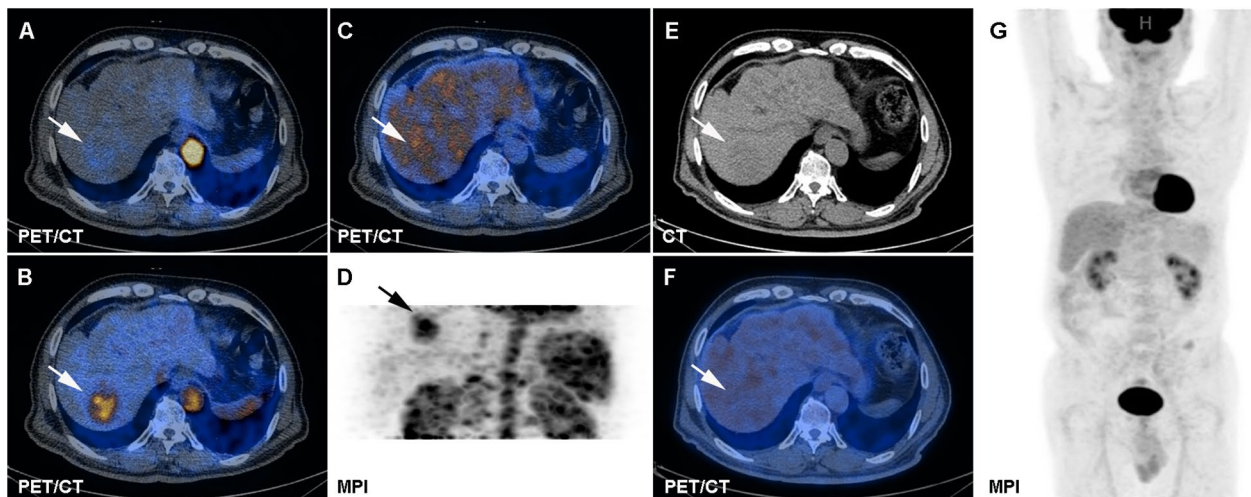


Fig. 2 A 67-year-old man with HCC in the right lobe of the liver. The postoperative pathological diagnosis was HCC (grade II), MVI (M0), and non-cirrhosis. Axial-fused ED ^{18}F -FDG PET/CT sequential blood flow images during **a** early arterial phase, **B** late arterial phase, and **c** venous phase and **d** MIP image show preferential arterial supply to HCC (arrow) versus background liver parenchyma.

For HCC and background liver parenchyma, TTPs were 18.11 and 59.51 s, respectively; BFs were 0.86 and 0.49 mL/min/g, respectively; and HPIs were 0.77 and 0.45, respectively. WB PET/CT: axial **e** CT, **f** fused PET/CT (arrows), and **G** PET MIP of the tumor show no increased FDG uptake in the HCC versus the background liver parenchyma (SUV_{max} = 4.2, TNR = 1.2)

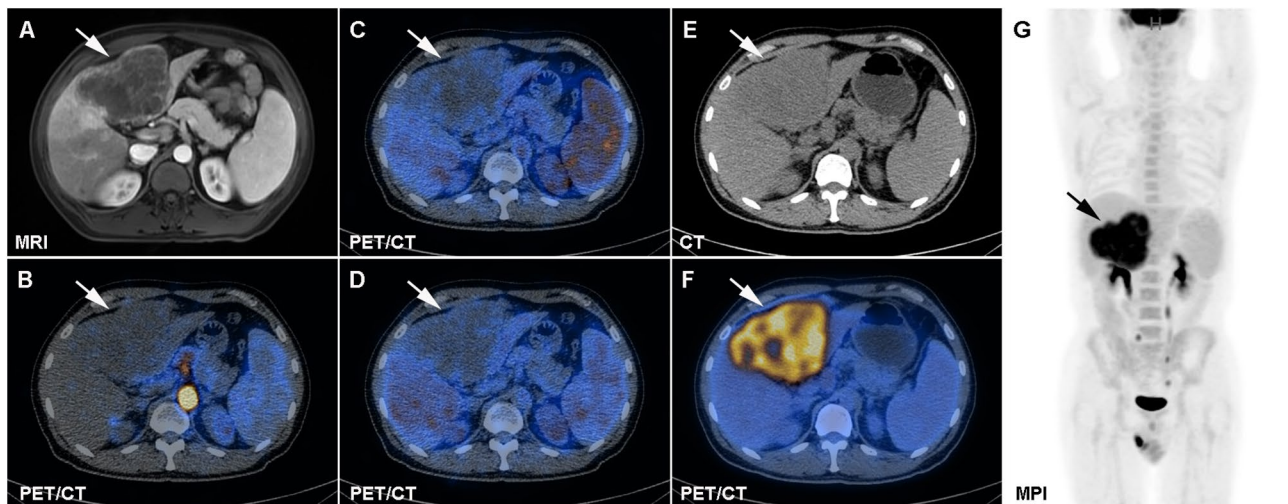


Fig. 3 A 51-year-old man with HCC in the left lobe of the liver. The postoperative pathological diagnosis was HCC (grade III), MVI (M2), and cirrhosis. **a** Axial enhanced MRI showed mild enhancement of the left lobe of liver tumor in the arterial phase (arrow). Axial-fused ED ^{18}F -FDG PET/CT sequential blood flow images during **b** early arterial phase, **c** late arterial phase, and **d** venous phase show no preferential arterial supply to HCC (arrow) ver-

sus background liver parenchyma. For HCC and background liver parenchyma, TTPs were 10.42 and 48.57 s, respectively; BFs were 0.33 and 0.51 mL/min/g, respectively; and HPIs were 0.90 and 0.48, respectively. WB PET/CT: axial **e** CT, **f** fused PET/CT, and **g** PET MIP (arrows) of the tumor show increased FDG uptake in the HCC versus the background liver parenchyma (SUVmax=15.4, TNR=6.2)

Quantitative analysis

TTP was shorter in HCC than in background liver ($34.99 \text{ s} \pm 16.52$ vs $54.09 \text{ s} \pm 15.36$; $t = -4.184$, $P < 0.001$) and HPI was higher in HCC than in background liver parenchyma (0.62 ± 0.15 vs 0.51 ± 0.10 ; $t = 2.993$, $P = 0.004$), but there was no significant difference in BF between HCC and background liver parenchyma ($0.60 \text{ mL/min/g} \pm 0.22$ vs $0.51 \text{ mL/min/g} \pm 0.10$; $t = 0.405$, $P = 0.687$). TTP was shorter in spleen than in HCC ($12.19 \text{ s} \pm 3.97$ vs $34.99 \text{ s} \pm 16.52$; $t = -7.050$, $P < 0.001$) and BF was higher in spleen than in HCC ($1.09 \text{ mL/min/g} \pm 0.30$ vs $0.60 \text{ mL/min/g} \pm 0.22$; $t = 6.655$, $P < 0.001$). SUVmax was significantly higher in HCCs than in background liver parenchyma (4.5 ± 2.9 vs 2.8 ± 0.5 ; $t = 2.855$, $P = 0.008$) (Table 1). The TNR value of HCC was 1.6 ± 1.1 .

HPI was higher in HCCs in patients with liver cirrhosis than those without liver cirrhosis (0.66 ± 0.16 vs 0.54 ± 0.08 ; $t = 2.211$, $P = 0.044$). There was no significant difference in TTP, BF, SUVmax, or TNR between HCCs in patients with liver cirrhosis and those without liver cirrhosis. There was no significant difference in blood flow estimates and SUVmax in background liver parenchyma between patients with and those without cirrhosis (Table 2).

In 24 HCCs, the presence of MVI (including M1 and M2) was confirmed histopathologically in 8 HCCs. TTP was shorter in HCCs with MVI than without MVI ($28.00 \text{ s} \pm 13.69$ vs $42.13 \text{ s} \pm 16.23$; $t = -2.110$, $P = 0.046$).

There was no significant difference in BF, HPI, SUVmax, or TNR between HCCs with MVI and without MVI. There was no significant difference in blood flow estimates and SUVmax in background liver parenchyma between patients with and those without MVI (Table 3).

Discussion

HCC is usually considered to be a blood-rich lesion and its occurrence is closely related to the increase of arterial blood supply, mainly related to tumor-related arterial neovascularization. The main blood supply of HCC comes from the hepatic artery and part of the blood supply comes from the portal vein; conversely, the blood supply of normal liver tissue comes mostly from the portal vein and a small part comes from the hepatic artery. At the same time, in the first pass, the time of peak arterial blood supply is before the portal vein. Therefore, TTP is a quantitative indicator that reflects the difference between liver lesions and liver background. Consistent with the results of previous studies [3], our data show that the TTP of HCC is shorter than the TTP of the background liver. HPI represents the percentage of arterial blood supply to the total liver blood flow. Compared with the background liver, the HPI of HCC is significantly higher. Our data also confirmed that the hepatic artery preferentially supplies HCC, suggesting that ^{18}F -FDG blood flow parameters may estimate the angiogenesis of liver cancer. In addition, our research also shows that the BF of HCC

Table 1 ^{18}F -FDG blood flow estimates and SUVmax in HCC, background liver, and spleen

	HCC (n=28)	Background liver (n=22)	Spleen (n=22)	P value		
				HCC vs liver	HCC vs spleen	Liver vs spleen
TTP	34.99 ± 16.52 (10.42–69.64)	54.09 ± 15.36 (20.48–77.76)	12.19 ± 3.97 (4.00–20.35)	<0.001	<0.001	<0.001
BF	0.60 ± 0.22 (0.16–0.97)	0.58 ± 0.17 (0.32–0.83)	1.09 ± 0.30 (0.71–1.78)	0.687	<0.001	<0.001
HPI	0.62 ± 0.15 (0.46–0.94)	0.51 ± 0.10 (0.42–0.91)		0.004		
SUVmax	4.5 ± 2.9 (1.7–15.4)	2.8 ± 0.5 (1.6–3.5)		0.008		

Bold values indicate statistically significant ($p < 0.05$)

Table 2 ^{18}F -FDG blood flow estimates and SUVmax of HCC and background liver in patients with and those without liver cirrhosis

	HCC			Background liver		
	Liver cirrhosis (n=11)	Non-liver cirrhosis (n=13)	P value	Liver cirrhosis (n=10)	Non-liver cirrhosis (n=9)	P value
TTP	36.21 ± 20.85 (10.42–69.64)	38.44 ± 12.74 (18.12–62.32)	0.761	55.30 ± 14.67 (31.39–77.76)	56.84 ± 11.84 (28.88–71.95)	0.806
BF	0.54 ± 0.21 (0.16–0.88)	0.64 ± 0.22 (0.34–0.97)	0.626	0.54 ± 0.18 (0.32–0.79)	0.59 ± 0.16 (0.38–0.83)	0.555
HPI	0.66 ± 0.16 (0.49–0.94)	0.54 ± 0.08 (0.46–0.77)	0.044	0.50 ± 0.04 (0.43–0.56)	0.49 ± 0.06 (0.42–0.62)	0.563
SUVmax	4.8 ± 3.7 (2.4–15.4)	4.0 ± 2.5 (1.7–11.3)	0.524	2.9 ± 0.3 (2.5–3.3)	2.9 ± 0.6 (1.6–3.5)	0.872
TNR	1.7 ± 1.5 (0.9–6.2)	1.4 ± 0.8 (0.8–3.6)	0.439			

Bold value indicates statistically significant ($p < 0.05$)

Table 3 ^{18}F -FDG blood flow estimates and SUVmax of HCC and background liver in patients with and those without MVI

	HCC			Background Liver		
	M1 + M2 (n=8)	M0 (n=16)	P value	M1 + M2 (n=8)	M0 (n=11)	P value
TTP	28.00 ± 13.69 (10.42–53.28)	42.13 ± 16.23 (18.12–69.64)	0.046	57.46 ± 13.55 (31.39–71.95)	55.00 ± 13.25 (28.88–77.76)	0.697
BF	0.58 ± 0.18 (0.33–0.88)	0.60 ± 0.24 (0.16–0.97)	0.817	0.59 ± 0.17 (0.34–0.80)	0.54 ± 0.17 (0.32–0.83)	0.554
HPI	0.68 ± 0.18 (0.51–0.94)	0.56 ± 0.08 (0.46–0.77)	0.087	0.49 ± 0.03 (0.42–0.91)	0.50 ± 0.06 (0.43–0.62)	0.681
SUVmax	6.6 ± 4.4 (2.3–15.4)	3.3 ± 1.0 (1.7–6.4)	0.068	2.7 ± 0.6 (1.6–3.3)	3.0 ± 0.3 (2.7–3.5)	0.238
TNR	2.5 ± 1.7 (1.4–6.2)	1.1 ± 0.3 (1.0–2.8)	0.060			

Bold value indicates statistically significant ($p < 0.05$)

is higher than the background liver and the SUVmax of HCC is higher than that of background liver.

It is known that liver cirrhosis can affect and alter liver vascularisation and hepatic circulation can differ with varying grades of cirrhosis [13]. The results of this study show

that there is no significant difference in BF between cirrhosis and non-cirrhosis background liver, which is consistent with Sørensen's conclusion [14]. The results of this study show that the HPI value of HCC in cirrhotic patients is higher than that of HCC in non-cirrhotic patients, but there is no

significant difference in TTP between them. Kwee et al. found no statistically significant difference in tumor SUV-max or TNR between cirrhotic and non-cirrhotic patients [15], which is consistent with the results of our study.

Our research shows that there are significant differences in TTP between HCC lesions with and without MVI, but the background liver blood parenchyma perfusion parameters are similar between the two groups. Huang et al. found large tumor size, irregular tumor margin, and peritumor enhancement in preoperative Gd-EOB-DTPA-dynamic enhanced MRI could predict the presence of MVI in HCC [16]. The irregular circumferential peritumor enhancement might represent a direct tumor-related hemodynamic change in the corona enhancement and/or the tumorous AP shunt [17]. It is likely due to the compensatory arterial hyperperfusion that occurred in the areas of decreased portal flow secondary to minute portal branch occlusion from tumor invasion [16]. Our data show that the SUVmax and TNR values of HCC with MVI are higher than those without MVI, but there is no statistical difference. The results of Hyun SH in European nuclear medicine showed that 76 of 158 HCC patients had MVI (48.1%). Multivariate logistic regression analysis showed that TNR, serum alpha-fetoprotein (AFP) levels, and tumor size were significantly correlated with the presence of MVI ($P < 0.001$). There was no significant correlation between multinodularity and MVI ($P = 0.563$) [18].

In the study, we found that the 6 lesions that were significantly enhanced in enhanced MRI or CT were not visually observed to have obvious FDG uptake in FDG dynamic imaging. The 6 lesions were 3 cases of moderately differentiated HCC and 3 cases of poorly differentiated HCC, with diameters ranging from 1.5 to 3 cm. The reason may be related to the following factors. (1) The resolution of the detector. Small lesions may be ignored; (2) the degree of tumor differentiation. Asayama proposed that HCC showed significantly different hemodynamic patterns between different histological grades [19]. Whether in radiology or pathology, the vascular distribution of poorly differentiated HCC is less than that of moderately differentiated HCC.

Our study has certain limitation. According to the literature, the average radioactivity of each time point of each VOI is fitted by the Gamma variable to generate a time radiation curve. Because the maximum radioactivity at each time point is relatively discrete, it is not easy to use the Gamma variable to fit the time–activity curve, so the average radioactivity is used. However, the use of average radioactivity may underestimate the peak time of tumor radioactivity, delay TTP, and reduce the BF value [4]. Technical developments in dynamic PET/CT such as 194-cm-long total-body PET/CT scanner (uEXPLORER) will enable estimations of tumor blood flow in the ED phase [20].

Conclusion

TTP was shorter in HCC than in background liver, HPI was higher in HCC than in background liver parenchyma, and ED combined WB ^{18}F -FDG PET/CT can significantly increase the detection rate of moderately differentiated and poorly differentiated HCC. HPI was significantly higher in HCCs in patients with liver cirrhosis than those without liver cirrhosis. TTP was significantly shorter in HCCs with MVI than without MVI.

Acknowledgements This study is supported by Science and Technology Committee of Shanghai Municipality (Grant No. 20DZ2201800), the Youth Medical Talents–Medical Imaging Practitioner Program of Shanghai “Rising Stars of Medical Talent” Youth Development Program (SHWRS (2020)_087), Special Fund for Clinical Research of Zhongshan Hospital, Fudan University (2020ZSLC63), and Shanghai Municipal Key Clinical Specialty (shslczdzk03401).

Declarations

Conflict of interest The authors declare no conflicts of interest.

References

- Villanueva A. Hepatocellular Carcinoma. *N Engl J Med*. 2019;380:1450–62.
- Kornberg A, Friess H. ^{18}F -fludeoxyglucose positron emission tomography for diagnosis of HCC: implications for therapeutic strategy in curative and non-curative approaches. *Therap Adv Gastroenterol*. 2019;12:1756284819836205.
- Bernstine H, Braun M, Yefremov N, Lamash Y, Carmi R, Stern D, et al. FDG PET/CT early dynamic blood flow and late standardized uptake value determination in hepatocellular carcinoma. *Radiology*. 2011;260:503–10.
- Schierz JH, Opfermann T, Steenbeck J, Lopatta E, Settmacher U, Stallmach A, et al. Early dynamic ^{18}F -FDG PET to detect hyperperfusion in hepatocellular carcinoma liver lesions. *J Nucl Med*. 2013;54:848–54.
- Wang SB, Wu HB, Wang QS, Zhou WL, Tian Y, Li HS, et al. Combined early dynamic ^{18}F -FDG PET/CT and conventional whole-body ^{18}F -FDG PET/CT provide one-stop imaging for detecting hepatocellular carcinoma. *Clin Res Hepatol Gastroenterol*. 2015;39:324–30.
- Freesmeyer M, Winkens T, Schierz JH. Contrast between hypervascularized liver lesions and hepatic parenchyma: early dynamic PET versus contrast-enhanced CT. *Ann Nucl Med*. 2014;28:664–8.
- Zhang X, Li J, Shen F, Lau WY. Significance of presence of microvascular invasion in specimens obtained after surgical treatment of hepatocellular carcinoma. *J Gastroenterol Hepatol*. 2018;33:347–54.
- Erstad DJ, Tanabe KK. Prognostic and Therapeutic Implications of Microvascular Invasion in Hepatocellular Carcinoma. *Ann Surg Oncol*. 2019;26:1474–93.
- Mullani NA, Herbst RS, O’Neil RG, Gould KL, Barron BJ, Abbruzzese JL. Tumor blood flow measured by PET dynamic imaging of first-pass ^{18}F -FDG uptake: a comparison with ^{15}O -labeled water-measured blood flow. *J Nucl Med*. 2008;49:517–23.
- Cochet A, Pigeonnet S, Khoury B, Vrigneaud JM, Touzery C, Berriolo-Riedinger A, et al. Evaluation of breast tumor blood flow with dynamic first-pass ^{18}F -FDG PET/CT: comparison

- with angiogenesis markers and prognostic factors. *J Nucl Med.* 2012;53:512–20.
11. Miles KA, Hayball P, Dixon AK. Functional images of hepatic perfusion obtained with dynamic CT. *Radiology.* 1993; 88: 405–11.
 12. Cong WM, Bu H, Chen J et al. Practice guidelines for the pathological diagnosis of primary liver cancer: 2015 update. *World J Gastroenterol.* 2016; 22: 9279–87.
 13. Azizah M Afif, Jason Pik-Eu Chang, Yan Y Wang, Simin D Lau, Fuzhen Deng, Shy Y Goh, et al. A sonographic Doppler study of the hepatic vein, portal vein and hepatic artery in liver cirrhosis: Correlation of hepatic hemodynamics with clinical Child Pugh score in Singapore. *Ultrasound.* 2017;25: 213–21.
 14. Sørensen M, Mikkelsen KS, Frisch K, Villadsen GE, Keiding S. Regional metabolic liver function measured in patients with cirrhosis by 2-[¹⁸F]fluoro-2-deoxy-D-galactose PET/CT. *J Hepatol.* 2013;58:1119–24.
 15. Kwee SA, Wong LL, Hernandez BY, Chan OT, Sato MM, Tsai N. Chronic Liver Disease and the Detection of Hepatocellular Carcinoma by [(18)F]fluorocholine PET/CT. *Diagnostics (Basel).* 2015;5:189–99.
 16. Huang M, Liao B, Xu P, Cai H, Huang K, Dong Z, et al. Prediction of Microvascular Invasion in Hepatocellular Carcinoma: Preoperative Gd-EOB-DTPA-Dynamic Enhanced MRI and Histopathological Correlation. *Contrast Media Mol Imaging.* 2018; 2018: 9674565.
 17. Kim H, Park MS, Choi JY, Park YN, Kim MJ, Kim KS, et al. Can microvessel invasion of hepatocellular carcinoma be predicted by pre-operative MRI? *European Radiology.* 2009;19:1744–51.
 18. Hyun SH, Eo JS, Song BI, Lee JW, Na SJ, Hong IK, et al. Pre-operative prediction of microvascular invasion of hepatocellular carcinoma using (18)F-FDG PET/CT: a multicenter retrospective cohort study. *Eur J Nucl Med Mol Imaging.* 2018;45:720–6.
 19. Asayama Y, Yoshimitsu K, Nishihara Y, et al. Arterial blood supply of hepatocellular carcinoma and histologic grading: radiologic-pathologic correlation. *AJR Am J Roentgenol.* 2008;190:W28–34.
 20. Zhang X, Xie Z, Berg E, et al. Total-Body Dynamic Reconstruction and Parametric Imaging on the uEXPLORER. *J Nucl Med.* 2020;61(2):285–291.

Publisher's Note Springer Nature remains neutral with regard to jurisdictional claims in published maps and institutional affiliations.

Springer Nature or its licensor (e.g. a society or other partner) holds exclusive rights to this article under a publishing agreement with the author(s) or other rightsholder(s); author self-archiving of the accepted manuscript version of this article is solely governed by the terms of such publishing agreement and applicable law.

Authors and Affiliations

Yiqiu Zhang^{1,2,3,4} · Yun Dong⁵ · Wenjun Yu⁵ · Shuguang Chen^{1,3,4} · Haojun Yu^{1,3,4} · Beilei Li^{2,3,4} · Hongcheng Shi^{1,2,3,4} 

✉ Beilei Li
li.beilei@zs-hospital.sh.cn

✉ Hongcheng Shi
shihongcheng163@163.com

¹ Department of Nuclear Medicine, Zhongshan Hospital, Fudan University, Shanghai, China

² Department of Nuclear Medicine, Zhongshan Hospital (Xiamen), Fudan University, Xiamen, Fujian, China

³ Nuclear Medicine Institute of Fudan University, Shanghai, China

⁴ Shanghai Institute of Medical Imaging, Shanghai, China

⁵ Shanghai United Imaging Healthcare Co., Ltd., Shanghai, China